Comparison of numerical methods for slug capturing with the two-fluid model

Maurice H.W. Hendrix[1], Ivar E. Smith[2], Joost S.B. van Zwieten[1], Benjamin Sanderse[3]

[1] *Delft University of Technology, Delft, The Netherlands*

[2] *NTNU, Trondheim, Norway*

[3] *Shell Technology Centre Amsterdam, Amsterdam, The Netherlands*

Abstract

In this paper the capability of the two-fluid model to describe the transition from stratified to slug flow is investigated, by employing three different numerical discretization techniques: classical finite volume, discontinuous Galerkin, and a Lagrangian finite volume approach. It is shown that stratified wavy flow can transition from well-posed to ill-posed following the Kelvin-Helmholtz instability mechanism. In the ill-posed regime grid convergence cannot be obtained. However, with low order discretization methods, or coarse grids and time steps, well-posed numerical solutions can still be obtained. Such solutions should however be critically assessed because they seem to be physical while in fact they are meaningless. The conditional well-posedness of the two-fluid model therefore requires a careful discretization in order to use it for slug capturing.

Keywords: two-fluid model, slug capturing, well-posedness, finite volume method

1. Introduction

In the petroleum industry multiphase flow occurs when transporting oil and gas through long multiphase pipeline systems. The behaviour of the flow can take many forms, depending on parameters like fluid velocities, pipe properties and fluid properties. An important flow regime is slug flow, in which liquid pockets, separated by gas bubbles, propagate in an alternating fashion with high speed along the pipeline. Such slugs have a large influence on the sizing of receiving facilities such as slug catchers or separators. The industry uses various flow models for simulating slug flow, but there is a need for increased accuracy. A promising approach is using so-called slug capturing, through the accurate numerical solution of the one-dimensional two-fluid model. This approach is believed to be capable of describing the transition from stratified flow to slug flow, see e.g. Ref. [1].

One of the issues in the transition from stratified flow to slug flow is that the two-fluid model can become ill-posed, see e.g. Ref. [2] and Ref [3]. Reference [2] mainly focuses on the effect of the spatial discretization and employs an incompressible model. Reference [3] also discusses the incompressible model and performs linear and nonlinear stability analyses. In this paper we instead consider the full compressible model and study several spatial and the temporal discretization methods and on ill-posedness and on convergence and stability. The paper is organized as follows: in section 2 the two-fluid model equations are explained, in section 3 the different discretization methods are presented, and in section 4 results are shown for the Kelvin-Helmholtz instability

2. Governing equations of the two-fluid model

The governing equations of the one-dimensional two-fluid model consist of a mass and momentum conservation equation for each phase:

$$\frac{\partial}{\partial t}\left(\rho_k A_k\right)+\frac{\partial}{\partial x}\left(\rho_k A_k u_k\right)=0 \tag{1}$$

$$\frac{\partial}{\partial t}\left(\rho_k A_k u_k\right)+\frac{\partial}{\partial x}\left(\rho_k A_k u_k^2\right)+A_k\frac{\partial p}{\partial x}+LG_k+\sum_{\substack{\gamma\in\{W,G,L\}\\ \gamma\neq k}} P_{k\gamma}\tau_{k\gamma} + A_k\rho_k g\sin\theta \;=0 \tag{2}$$

supplemented with the constraint $\sum_k A_k = A$. Here A_k is the is cross-sectional area occupied by phase k. The density and the velocity of phase k are denoted by ρ_k and u_k respectively. LG_k represents the hydraulic level gradient term, which can be expressed in conservative form by integrating the hydrostatic pressure over the cross-sectional phase area A_k. The level gradient term for the gas and liquid phase will thus read (van Zwieten et al., Ref [4]):

$$\mathrm{LG}_k=\frac{\partial}{\partial x}\left(\rho_k g\cos\theta(hA_k\pm\frac{1}{12}P_{LG}^3)\right) \tag{3}$$

Note that this model is more complete than the one in Ref. [2] since we take compressibility into account in all terms, including the level gradient term.

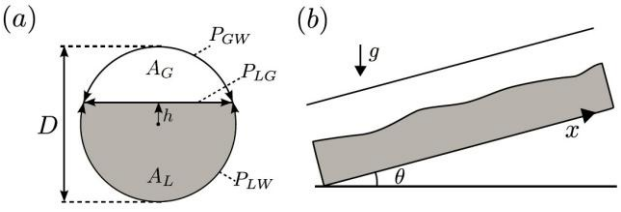

Figure 1: Schematic two-phase stratified pipe flow. (a) The cross-section shows the definition of the perimeters and the interface height h which is defined relative to the pipe center. (b) Cross-section indicating the pipe coordinate x and inclination angle θ.

We assume an isothermal system, so that the density of the gas and liquid phases are given by an equation of state which is a function of pressure only.

2.1. Friction models

The wall and interfacial shear stress are expressed by the Fanning friction factor definition:

$$\tau_{k\gamma} = \begin{cases} \frac{1}{2} f_k \rho_k u_k \mid u_k \mid & \text{if } \gamma = W \\ \frac{1}{2} f_{int} \rho_G \left(u_k - u_\gamma\right) \mid u_k - u_\gamma \mid & \text{if } \gamma \in \{G, L\} \end{cases} \tag{4}$$

We model the friction factor f_k of phase k with the pipe wall with Churchill's relation (Ref [5]):

$$f_k = 2\left(\left(\frac{8}{\mathrm{Re}}\right)^{12} + (A+B)^{-1.5}\right)^{\frac{1}{12}}$$
$$A = \left(2.457 \ln\left(\left(\left(\frac{7}{\mathrm{Re}_k}\right)^{0.9} + 0.27\frac{\varepsilon}{D_{hk}}\right)^{-1}\right)\right)^{16} \tag{5}$$
$$B = \left(\frac{37530}{\mathrm{Re}_k}\right)^{16}$$

Here ε is the hydraulic pipe roughness, Re_k is the Reynolds number,

$$\mathrm{Re}_k = \frac{\rho_k u_k D_{hk}}{\mu_k} \tag{6}$$

and D_{hk} is the hydraulic diameter:

$$D_{hk} = \begin{cases} \frac{4A_L}{P_{LW}} & \text{if } k = \mathrm{L} \\ \frac{4A_G}{P_{GW} + P_{GL}} & \text{if } k = \mathrm{G} \end{cases} \tag{7}$$

The interfacial friction factor f_{int} is calculated by:

$$f_{int} = \max\{f_G, 0.014\} \tag{8}$$

3. Discretization techniques

Three different numerical discretization techniques are investigated in this paper: classical finite volume (CFV), discontinuous Galerkin (DG), and a Lagrangian finite volume (LFV) approach. The discontinuous Galerkin method combines features of both finite element and finite volume methods. The CFV and LFV methods share many similarities, though several aspects like discretization, solution procedure and pressure-velocity coupling are treated differently. The LFV model is also capable of employing moving control volumes, though this aspect of the model is not of primary focus in this study and is thus not described in the LFV model description. All three models employ a staggered grid, illustrated in Figure 2.

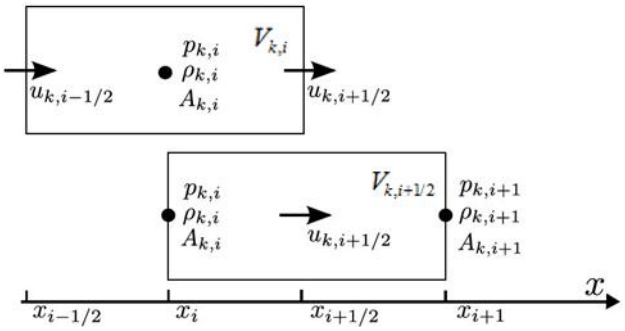

Figure 2: Staggered grid lay-out that is used for the finite volume schemes.

The discrete equations for the mass and momentum equations of the three aforementioned models are presented in the following sections. Super-script n will be used to denote the time index, sub-script i represents the spatial index, while sub-script k represents the gas or liquid phase. A "hat" symbol (^) is placed above unknown new variables where a convection scheme like upwind or central difference is used.

3.1. Classical Finite Volume (CFV)

In this section the discretization of the classical finite volume approach will be explained. First the spatial discretization is discussed, followed by the temporal discretization. Finally, the interpolation of unknown quantities is discussed.

Mass conservation equation:

The mass conservation equation is discretized by integrating Eqn (1) over the p-volume $V_{k,i}$. In our 1D framework this results in an integral in the x-direction which yields:

$$\frac{d}{dt}\left(\rho_{k,i} V_{k,i}\right) + (\rho A)_{k,i+1/2} u_{k,i+1/2} - (\rho A)_{k,i-1/2} u_{k,i-1/2} = 0 \tag{9}$$

Momentum conservation equation:

In a similar way we integrate Equation (2) over the u-volume ($V_{k,i+1/2}$) to obtain

$$\begin{aligned} &\frac{d}{dt}\left(\rho_{k,i+1/2} u_{k,i+1/2} V_{k,i+1/2}\right) + (\rho A)_{k,i+1} (u_{k,i+1})^2 - (\rho A)_{k,i} (u_{k,i})^2 \\ &+ A_{k,i+1/2}\left(p_{i+1} - p_i\right) + \mathrm{LG}_{k,i+1/2} \\ &+ \sum_{\substack{\gamma \in \{\mathrm{G,L,W}\} \\ \gamma \neq k}} P_{k\gamma,i+1/2} \tau_{k\gamma,i+1/2} \Delta x_{i+1/2} + \rho_{k,i+1/2}\, g \sin\theta\, V_{k,i+1/2} = 0 \end{aligned} \tag{10}$$

$\mathrm{LG}_{k,i+1/2}$ is the discrete level gradient. For the gas phase the discrete level gradient is calculated as:

$$\mathrm{LG}_{\mathrm{G},i+1/2} = g\cos\theta\left(\rho_{\mathrm{G},i+1}\left(hA_{\mathrm{G}} + \frac{P_{LG}^3}{12}\right)_{i+1} - \rho_{\mathrm{G},i}\left(hA_{\mathrm{G}} + \frac{P_{LG}^3}{12}\right)_i\right) \tag{11}$$

The level gradient of the liquid phase is approximated in a similar fashion. For the central scheme, the unknown variables are calculated by:

$$\hat{\phi}_{i,\mathrm{CD}} = \frac{1}{2}\left(\phi_{i-\frac{1}{2}} + \phi_{i+\frac{1}{2}}\right), \quad \hat{\phi}_{i+\frac{1}{2},\mathrm{CD}} = \frac{1}{2}\left(\phi_i + \phi_{i+1}\right) \tag{12}$$

For the FOU scheme, any unknown variable ϕ is taken from the direction the flow is coming. Since the velocities are all positive in the current test case, we get:

$$\hat{\phi}_{i,\mathrm{FOU}} = \phi_{i-\frac{1}{2}}, \quad \hat{\phi}_{i+\frac{1}{2},\mathrm{FOU}} = \phi_i \tag{13}$$

Time integration:

In order to advance the two-fluid model in time, a composite vector $\boldsymbol{U}$ which contains mass and momentum at all grid points is created. If we define $M_{k,i} \equiv \rho_{k,i} V_{k,i}$ and $P_{k,i+1/2} \equiv \rho_{k,i+1/2} u_{k,i+1/2} V_{k,i+1/2}$, this vector, for N grid points, will have the form:

$$\begin{aligned}\boldsymbol{U} = [&M_{(G,1)},\ldots,M_{(G,N)},M_{(L,1)},\ldots,M_{(L,N)},\\ &P_{(G,1+1/2)},\ldots,P_{(G,N+1/2)},P_{(L,1+1/2)},\ldots P_{(L,N+1/2)}]^T\end{aligned} \tag{14}$$

The complete semi-discrete system can be then written as:

$$\frac{d\boldsymbol{U}}{dt} = F(\boldsymbol{U}) \tag{15}$$

In this formulation we substituted the constraint to close the system. The temporal discretization used for the classical finite volume scheme is a BDF scheme:

$$\frac{1}{\Delta t}\left(a_0 \boldsymbol{U}^{n+1} + a_1 \boldsymbol{U}^{n} + a_2 \boldsymbol{U}^{n-1}\right) = \beta F(\boldsymbol{U}^{n+1}) \tag{16}$$

We will consider two BDF schemes. The first one is a BDF1 scheme, which is essentially a backward Euler scheme. For BDF1 the coefficients read: $a_0 = 1$, $a_1 = -1$, $a_2 = 0$ and $\beta = 1$. The second scheme we consider is the second order BDF2 scheme with coefficients $a_0 = 1, a_1 = -4/3,\ a_2 = 1/3$ and $\beta = 2/3$.

For both the BDF1 and BDF2 scheme Eqn (16) constitutes a nonlinear system that needs to be solved for $\boldsymbol{U}^{n+1}$, which we achieve by using a Newton approach. The fact that the system is solved for $\boldsymbol{U}^{n+1}$, which contains the mass and momentum at each grid point, guarantees mass and momentum conservation independent of time step and grid size.

3.2. Lagrangian Finite Volume (LFV)

The LFV code is also a finite volume method, like the CFV code, but features some distinct differences:

- Possibility to use moving control volumes (not used in the current study).
- The constraint is implemented via a pressure equation.
- The squared velocity in the convective momentum term consists of one central interpolation multiplied by a selected convection scheme, like first order upwind. The CFV model on the other hand uses the squared value of the selected convection scheme.

Mass conservation equation:

$$\frac{M_{k,i}^{n+1} - M_{k,i}^{n}}{\Delta t} = \hat{m}_{k,i-1/2}^{n+1} A_{i-1/2}^{n} u_{k,i-1/2}^{n+1} - \hat{m}_{k,i+1/2}^{n+1} A_{i+1/2}^{n} u_{k,i+1/2}^{n+1} \tag{17}$$

Here, m_k is the specific mass, defined by:

$$m_k = \rho_k \alpha_k = \frac{M_k}{V} \tag{18}$$

while α_k and V are the hold-up fractions and total cell volume respectively.

Momentum conservation equation:

The momentum equation is solved for the change in velocity:

$$\begin{aligned}&M_{k,i+1/2}^{n} \frac{u_{k,i+1/2}^{n+1} - u_{k,i+1/2}^{n}}{\Delta t} + \frac{M_{k,i+1/2}^{n+1} - M_{k,i+1/2}^{n}}{\Delta t} u_{k,i+1/2}^{n+1}\\ &\quad + m_{k,i+1}^{n+1} A_{i+1}^{n} u_{k,i+1}^{n+1} \hat{u}_{k,i+1}^{n+1} - m_{k,i-1}^{n+1} A_{i-1}^{n} u_{k,i-1}^{n+1} \hat{u}_{k,i-1}^{n+1} =\\ &\quad -V_{k,i+1/2}^{n} \frac{\left(p_{i+1}^{n+1} - p_{i-1}^{n+1}\right)}{\Delta x_{k,i+1/2}^{n}} - \Delta x_{k,i+1/2}^{n} L G_k^{n}\\ &\quad -\tau_{kW,i+1/2}^{n} P_{kW,i+1/2}^{n} \Delta x_{k,i+1/2}^{n} - \tau_{GL,i+1/2}^{n} P_{GL,i+1/2}^{n} \Delta x_{k,i+1/2}^{n}\\ &\quad -M_{k,i+1/2}^{n} g \sin\theta\end{aligned} \tag{19}$$

The level gradient term is discretized identical to what is done in the CFV method.

Time integration and pressure-velocity coupling:

In contrast to the CFV code, the LFV code implements the constraint by deriving a pressure equation. This equation is obtained by expanding the time derivative of mass in the continuous mass equation, Eqn (1), by the product rule, dividing by the fluid density and summing this equation over all phases:

$$\sum_k \frac{V_{k,i}^{n+1}}{\rho_{k,i}^{n}} \left[\left(\frac{\partial \rho_{k,i}^{n}}{\partial p}\right)_T\right] \frac{p_i^{n+1} - p_i^{n}}{\Delta t} = \sum_k \left(\frac{1}{\rho_{k,i}^{n}} \begin{bmatrix} \hat{m}_{k,i-1/2}^{n+1} A_{i-1/2}^{n} u_{k,i-1/2}^{n+1} \\ -\hat{m}_{k,i+1/2}^{n+1} A_{i+1/2}^{n} u_{k,i+1/2}^{n+1} \end{bmatrix}\right) + \Psi_i^{n} \tag{20}$$

The term Ψ_i^n represents a correction for a possible volume fraction error from the previous time step:

$$\Psi_i^{n} = \frac{\sum_k \frac{M_{k,i}^{n}}{\rho_{k,i}^{n}} - V_i^{n}}{\Delta t^{n+1}} \tag{21}$$

The momentum equation (Eqn (19)) first is solved for the change in velocity, using Eqn (20) to eliminate the unknown new pressure directly by substitution. After the momentum equation has been solved, the new velocity is inserted in the pressure equation (Eqn (20)) to obtain the change in pressure. The mass equation is then solved for the change in mass, and the procedure is repeated the volume fraction error (deviation from 1 in the sum of hold-up fractions) drops below 1e-8 in all simulations.

3.3. Discontinuous Galerkin (DG)

The third discretization scheme is the space-time Discontinuous Galerkin Finite Element Method (short DG) described in Ref [4]. A DG scheme is similar to a (continuous) Finite Element scheme with the notable exception that basis functions are discontinuous at element edges. This enables the use of stabilization mechanisms developed for Finite Volume schemes and naturally allows for nonconforming meshes. Due to being part of the family of Finite Element Methods it is relatively easy to construct a high-order scheme by increasing the order of the basis functions.

In this paper we use a third-order, piecewise polynomial basis in both space and time, which gives a fourth-order accurate scheme for linear pde's or non-linear pde's with sufficiently smooth solutions. We use a structured, equidistant mesh with rectangular elements encompassing the complete space-time domain. Due to the structure of the mesh and causality in time, it is not necessary to solve the discrete problem on the complete mesh at once. Instead we separate the mesh in a sequence of time-slabs consisting of all elements with the same time interval and solve the discrete problem per time-slab, starting with the first. Note that this procedure is very similar to the time stepping methods used for the Finite Volume schemes, with the difference that with DG a solution is obtained for an entire time-slab at once while with the Finite Volume schemes a solution is obtained at a single point in time per iteration.

The stabilization method is adaptation of Roe's method: as a reference state for linearization we use the average solution value at the element edges and the eigenvalue problem is solved numerically. The complete non-linear discrete system for one time-slab is solved using Newton's method and the linear subproblem using a sparse, direct solver. For more details we refer the reader to van Zwieten et al. (Ref [4]).

4. Results

4.1. Introduction

The test case we discuss considers the evolution of stratified flow to slug flow according to the Kelvin-Helmholtz instability mechanism, and is the same as described in the study by Liao et al. (Ref [2]) and van Zwieten et al. (Ref [4]). We investigate the effect of the different discretization methods on the growth of an initially smooth wave.

The pipeline and fluid properties are given in Table 1. L is the pipe length, D is the inner pipe diameter, θ is the pipe inclination and ε the pipe roughness.

Table 1: Pipeline and fluid properties.

L	D	θ	ε	ρ_l	μ_g	μ_l
[m]	[m]	[°]	[m]	[kg/m^3]	Pa·s	Pa·s
1	0.078	0	1e-8	1000	1.8e-5	8.9e-4

The liquid phase is assumed to be incompressible with density ρ_l. The density of the gas phase is given by:

$$\rho_G = \frac{p\rho_{ref}}{p_{ref}}, \tag{22}$$

where p_{ref} and ρ_{ref} are 10^5 Pa and 1.1614 kg/m^3 respectively.

The initial condition is a sinusoidal wave with the mean value and amplitude for the primitive variables listed in Table 2. The wave number is $k = 2\pi\ m^{-1}$ and the angular frequency ω is approximately 8.484 s^{-1}. For more information we refer to van Zwieten et al. (Ref [4]).

Table 2: Initial conditions.

$u_{G,\text{mean}}$	$u_{G,\text{amp}}$	$u_{L,\text{mean}}$	$u_{\text{L,amp}}$	$\alpha_{l,\text{mean}}$	$\alpha_{l,\text{amp}}$	P_{mean}	P_{amp}
[m/s]	[m/s]	[m/s]	[m/s]	[-]	[-]	[Pa]	Pa
13.82	0.25	1	7e-3	0.5	0.01	10^5	3.7

The mean values were computed by choosing the gas velocity and liquid holdup, and computing the resulting liquid velocity and pressure gradient from the steady state momentum balance obtained by combining the gas and liquid momentum equations, eliminating the pressure gradient (balancing friction and gravity). These initial values result in a required pressure gradient of 74.23 Pa/m, which was added as driving force (source term) to the momentum equations. Periodic boundary conditions are applied.

By computing the characteristic roots of the system of mass and momentum equations, the following well-posedness criterion can be obtained:

$$\left(u_G - u_L\right)^2 < \left(\frac{\alpha_L}{\rho_L} + \frac{\alpha_G}{\rho_G}\right)\frac{\rho_L - \rho_G}{\frac{\partial \alpha_l}{\partial h_l}} g\cos(\theta) \tag{23}$$

This criterion is identical to the Inviscid Kelvin-Helmholtz criterion (IKH) derived by Barnea and Taitel (Ref [6]), and gives the inviscid limit at which the two-fluid model becomes ill-posed (characteristic roots becomes complex).
According to Eqn (23), the test case is well-posed at the initial conditions specified in Table 2. However, a more detailed eigenvalue analysis shows that the initial condition is in the (viscous) well-posed unstable region, and consequently the initial perturbations will grow.

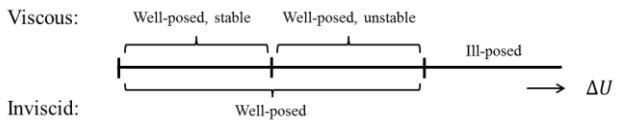

Figure 3: Schematic of stability and well-posedness limits for the two-fluid model.

4.2. Convergence behaviour in well-posed and ill-posed regions

Simulations were run with the different codes, with 40, 80 and 160 grid cells. The time step for each grid is calculated based on the CFL criterion for the liquid velocity: $\Delta t = \text{CFL}_\text{L}\frac{\Delta x}{u_L}$. The liquid CFL number (CFL_L) was calculated to be approximately 0.9875, based on the initial wave number and angular

frequency, so that we get an integer cycle of the sinusoidal wave after each 60 time steps.

On the left side of Figure 4 the liquid hold-up at different time instances is shown, corresponding to 1, 4 and 7 cycles of the wave moving through the domain. In black the exact analytical solution to the linearized system is added as a reference (note that this is only valid for small times). On the right side two of the four eigenvalues of the two-fluid model are shown (the other two correspond to fast pressure waves associated with acoustics, which are of less importance here). It can be seen that when time increases, the amplitude of the hold-up wave starts to grow. In Figure 4 (a) and (b) we clearly see convergence upon mesh refinement. We also observe that the higher order methods are much more accurate, although a fair comparison requires that we take into account the effect of computational time. In Figure 4 (c) the wave steepens and nonlinear effects are important. It can be seen that in the neighbourhood of the steepening, the real part of the eigenvalues are becoming equal. Closer inspection reveals that the eigenvalues are forming a complex conjugate pair. This indicates that the two-fluid model is not hyperbolic anymore and it therefore becomes ill-posed; Eqn (23) is violated. Related to this is that in the ill-posed region the different discretizations do not converge upon mesh refinement. This means that in essence the results of the two-fluid model have become meaningless. It can be noted that the fourth-order DG scheme already shows ill-posedness for the medium grid N=80, while the other schemes are still well-posed for N=80.

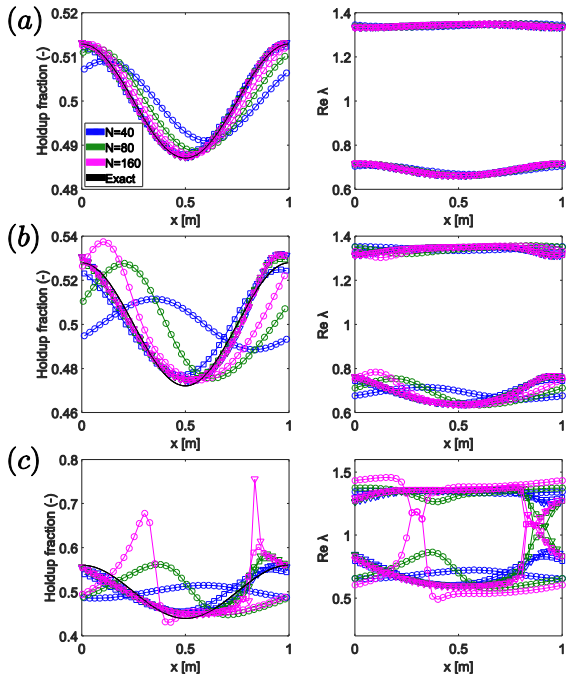

Figure 4: Wave evolution in terms of liquid hold-up and real part of eigenvalues after (a) 1, (b) 4 and (c) 7 cycles. LFV results are depicted with circles (○), CFV (BDF2) results are depicted with squares (□), and DG results are depicted with triangles (▽).

4.3. Influence of discretization method on predicting ill-posedness

We further investigate the effect of the discretization on ill-posedness by comparing the time instance at which complex eigenvalues first appear, t_C. For this study we focus on different discretization techniques using solely the CFV scheme. Figure 5 shows that, when the time step goes to zero, all methods converge towards the same t_C. Note that the grid is refined simultaneously with the time step since the CFL number is kept fixed.

When the time step increases, we observe that the lowest order methods start to deviate first. t_C rapidly increases, until a time step is reached for which complex eigenvalues are not found anymore. For time steps larger than this critical time step the simulations are well-posed, even though a refined – and therefore more accurate – simulation would indicate an ill-posed problem.

It is clear that this is an undesirable situation, since one can obtain seemingly meaningful results with a coarse grid or a low order discretization method, that are in fact meaningless. The advantage of higher order methods such as BDF2 instead of BDF1 (Backward Euler) is very clear here: with BDF2 we still obtain the 'correct' ill-posedness at time steps and grid sizes that are around 10 times larger than with BDF1. The advantage of BDF2 is not only apparent in terms of improved accuracy, but also, and maybe more importantly, in capturing the correct mathematical properties of the two-fluid model.

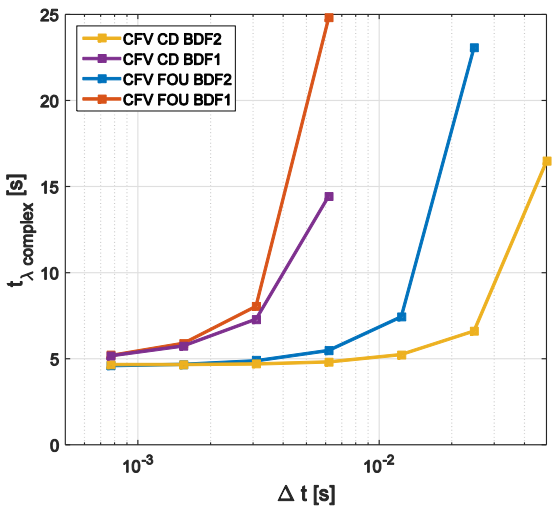

Figure 5: Time instance at which complex eigenvalues first appear, as function of time step, for different discretization methods.

5. Conclusions

In this paper we have investigated the growth of waves in stratified flow as a model for the transition of stratified flow to slug flow in multiphase flow pipelines. In particular, we have studied the effect of different discretization methods on the wave growth and on the onset of ill-posedness.

By studying the behaviour of the eigenvalues of the system of equations in space and time, it appears that during wave steepening the eigenvalues become complex. When simultaneously refining grid and time step, subsequent solutions

do not converge, i.e. they do not become grid independent when the eigenvalues are complex. However, given the same initial conditions, well-posed solutions can still be obtained when using low order discretization methods or coarse grids or time steps, although this is undesirable.

The current paper therefore indicates that initially well-posed, but unstable, waves in a stratified flow can grow to become ill-posed, before they have reached the top of the pipe, i.e. before stratified flow has transitioned to slug flow. This indicates that the transition from stratified flow to slug flow, at least for the conditions investigated in this paper, cannot be captured with the two-fluid model, since the model becomes ill-posed. The ill-posedness of the model manifests itself in a lack of convergence upon grid and time step refinement, which essentially renders the simulation results in the ill-posed regime useless. We have shown in this paper that, depending on the discretization method employed, well-posed solutions might still be obtained when using low order discretizations or coarse grids, as typically used in practical studies with commercial simulators. Such solutions should however be critically assessed because they can appear to be physical while in fact they are meaningless.

A number of options are available in literature to circumvent the ill-posedness of the two-fluid model, e.g. the inclusion of surface tension, axial diffusion, a virtual mass force, or a momentum flux parameter. For future work we recommend to investigate the effect of such terms on the transition from stratified to slug flow.

6. References

1. Issa, R.I. and M.H.W. Kempf, *Simulation of slug flow in horizontal and nearly horizontal pipes with the two-fluid model.* International Journal of Multiphase Flow, 2003. **29**(1): p. 69-95.
2. Liao, J., R. Mei, and J.F. Klausner, *A study on the numerical stability of the two-fluid model near ill-posedness.* International Journal of Multiphase Flow, 2008. **34**(11): p. 1067-1087.
3. Fullmer, W.D., V.H. Ransom, and M.A. Lopez de Bertodano, *Linear and nonlinear analysis of an unstable, but well-posed, one-dimensional two-fluid model for two-phase flow based on the inviscid Kelvin–Helmholtz instability.* Nuclear Engineering and Design, 2014. **268**: p. 173-184.
4. van Zwieten, J.S.B., B. Sanderse, M.H.W. Hendrix, C. Vuik, and R.A.W.M. Henkes, *Efficient simulation of one-dimensional two-phase flow with a new high-order Discontinuous Galerkin method*. 2015, Delft University of Technology.
5. Churchill, S., *Friction-factor equation spans all fluid-flow regimes.* Chemical Engineering, 1977. **84**(24): p. 91-92.
6. Barnea, D. and Y. Taitel, *Interfacial and structural stability of separated flow.* International Journal of Multiphase Flow, 1994. **20**: p. 387-414.